



HAL
open science

The geometry of Strombolian explosions: insights from Doppler radar measurements

Mathieu Gouhier, Franck Donnadieu

► **To cite this version:**

Mathieu Gouhier, Franck Donnadieu. The geometry of Strombolian explosions: insights from Doppler radar measurements. *Geophysical Journal International*, 2010, pp.1376-1391. 10.1111/j.1365-246X.2010.04829.x . hal-00576072

HAL Id: hal-00576072

<https://hal.science/hal-00576072>

Submitted on 18 Jun 2021

HAL is a multi-disciplinary open access archive for the deposit and dissemination of scientific research documents, whether they are published or not. The documents may come from teaching and research institutions in France or abroad, or from public or private research centers.

L'archive ouverte pluridisciplinaire **HAL**, est destinée au dépôt et à la diffusion de documents scientifiques de niveau recherche, publiés ou non, émanant des établissements d'enseignement et de recherche français ou étrangers, des laboratoires publics ou privés.

The geometry of Strombolian explosions: insights from Doppler radar measurements

Mathieu Gouhier^{1,2,3} and Franck Donnadieu^{1,2,3}

¹Clermont Université, Université Blaise Pascal, Laboratoire Magmas et Volcans, BP 10448, F-63000 Clermont-Ferrand, France.

E-mail: M.Gouhier@opgc.univ-bpclermont.fr

²CNRS, UMR 6524, LMV, F-63038 Clermont-Ferrand, France

³IRD, R 163, LMV, F-63038 Clermont-Ferrand, France

Accepted 2010 September 27. Received 2010 September 24; in original form 2009 May 27

SUMMARY

Observations of Strombolian volcanic explosions were carried out at Etna's southeast crater on 2001 July 4 using a ground-based pulsed Doppler radar (VOLDORAD). To obtain quantitative constraints on the geometry of the explosions, we modelled synthetic Doppler spectra by combining the outputs of a ballistic model to compute the theoretical velocities of gas and particles, and an electromagnetic scattering model to calculate the synthetic echo power. This allowed us to reproduce the shapes of recorded Doppler spectra for each volcanic explosion. We examined the geometrical distribution of ejected pyroclasts for about 200 explosions and found two main types of explosion, each showing a distinctive spectral signature. The first type, characterized by the triangular shape of their Doppler spectra, represents 34 per cent of the explosions. This spectrum shape is related to a Gaussian distribution of the pyroclast ejection angles, where most of the volcanic material is ejected vertically within a narrow cone, with the particle concentration decreasing radially. The second type represents about 12 per cent of the explosions, and is characterized by a top-hat-shaped spectrum. It is produced by a uniform distribution of pyroclast ejection angles. In this case, the bubbles tend to burst above the crater rim and eject the ballistic clasts hemispherically without preferential orientation. The majority of the Strombolian explosions analysed (54 per cent) are intermediate between these end-member shapes, and show a triangular spectra truncated by a plateau. They result from a uniform distribution of ejection angles around the jet axis.

The continuous radar recordings allowed us to carry out a statistical analysis on the geometrical features of the same 200 Strombolian explosions. Thus we find that 40° is a statistically representative aperture of the dispersion cone characterized by uniform ejecta distribution for explosions having a plateau component (i.e. 2/3 of all explosions studied). We also find that 80 per cent of the total particle load remains within this 40° dispersion cone, which in our case is oriented nearly vertically. Such quantification of the geometrical features of Strombolian explosions can provide constraints on shallow conduit processes. For example, the time evolution of the top-hat Doppler spectra during the paroxysm suggests that the magma level varies over a 15 min timescale.

Key words: Time-series analysis; Numerical approximations and analysis; Explosive volcanism; Eruption mechanisms and flow emplacement; Remote sensing of volcanoes; Volcano monitoring.

1 INTRODUCTION

Geometrical features of a volcanic explosion visible at the surface often provide information on the deeper mechanisms at the origin of the eruptive dynamics. Therefore, the acquisition of quantitative data on the geometrical characteristics of Strombolian jets is important in understanding the dynamics of this type of activity.

Acquisition of geometrical data is difficult because of the multiple parameters involved in the fast-evolving mechanism of particle ejection, and their complex rapid interactions and variability. In particular, the particle size distribution (PSD) may vary widely from one explosion to another and is very challenging to assess precisely during the dynamic stage and over the full range of particle sizes. The analysis of the kinetics of gas and ejecta and their geometric

evolution during Strombolian explosions requires high sampling rate devices capable of continuous monitoring of the surface activity, such as ground-based remote sensing methods. Photoballistic measurements have been carried out on Strombolian eruptions (Chouet *et al.* 1974; McGetchin *et al.* 1974; Blackburn *et al.* 1976; Ripepe *et al.* 1993), as well as on more explosive activity (Formenti *et al.* 2003). They provided quite accurate geometrical data, but only on a very small number of explosions. Such photoballistic analyses involve heavy and tedious work that would make it very difficult to carry out a statistical analysis of a whole series of Strombolian explosions. Weill *et al.* (1992) also attempted to give dynamic constraints, such as vertical velocities and PSDs, on Strombolian explosions using acoustic methods. More recently, thermal (Patrick 2007; Patrick *et al.* 2007) and UV (Mori & Burton 2009) cameras have provided insights into the morphology and dynamics of Strombolian explosions, and have led to a basic classification of Strombolian events. Thermal methods are very effective for assessing gas and ash plume dynamics, as they allow high sampling rate monitoring for a low detection threshold. Hort *et al.* (2003) used measurements from frequency-modulated continuous-wave Doppler radars to obtain geometric information for Stromboli volcano, which showed a nearly vertical orientation of lava jets for a large number of Strombolian events. Doppler radar measurements are well suited to this detailed and quantitative analysis of the surface eruptive activity since they are capable of providing a high sampling rate which is sustainable over long acquisition periods, provided the multiple parameters influencing the shape of Doppler radar spectra are correctly interpreted.

The aim of this paper is to define and constrain parameters from Doppler spectra recorded by VOLDORAD, a volcanological Doppler radar designed at the Observatoire de Physique du Globe de Clermont-Ferrand (OPGC, France) in order to improve constraints on the geometrical properties of Strombolian jets. The information held in volcanic Doppler spectra is complex, as it integrates simultaneously several kinetic, loading and geometric factors such as, for instance, the ejection angle distribution (EAD), sometimes called collimation, and the PSD. Therefore even a thorough inspection of the Doppler spectra is not sufficient to constrain the dynamics of Strombolian jets. Thus we combine here a ballistic model that gives the synthetic particle velocities, and an electromagnetic scattering model which provides the synthetic power backscattered by particles inside the radar sampling volumes in order to model synthetic Doppler spectra. We performed parametric tests to determine the main factors controlling the shape of radar spectra and their respective influence. We then use the analysis from two contrasted Strombolian explosions from Etna's SE crater during the 2001 July 4 eruption as detailed examples of the method developed here to retrieve their geometrical properties. Finally, we extend this method to a series of Strombolian explosions occurring during the paroxysm of this same eruption and compile a statistical dataset of their geometrical features.

2 RECORDED VOLCANO DOPPLER SPECTRA

2.1 Data acquisition with VOLDORAD

VOLDORAD is a pulsed Volcano Doppler Radar designed at the Observatoire de Physique du Globe de Clermont-Ferrand (France) for the study of explosive eruptions. The radar version used for the 2001 Etna campaign (VOLDORAD 2) operates at a wavelength of

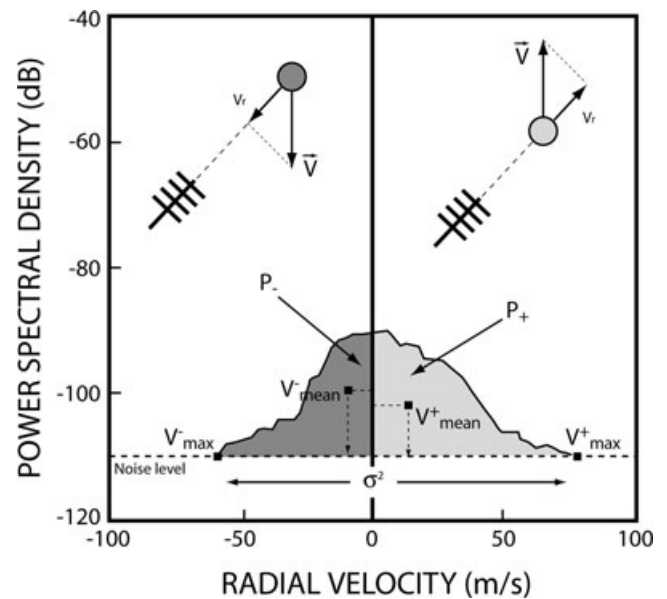


Figure 1. Main parameters of a typical volcanic Doppler spectrum, as calculated by the radar: power, maximum and mean radial velocities and spectral width. (+) and (–) indexes are for ejecta with the radial component of their velocity vector moving away from and towards the antenna, respectively.

23.5 cm (1278 MHz) and with a beam aperture of 9° . It records radial velocities and the backscatter of power from particles crossing the antenna beam in successive sampling volumes (termed range gates). Doppler spectra are computed in real time by a Fourier transform to obtain the energy distribution in the frequency domain from the digitized echo signal in the time domain. Radial velocities are determined from the Doppler shift; the distribution of the spectrum amplitude defines the power spectral density. Both parameters can subsequently be used to characterize the jet dynamics. Different values of the pulse duration, pulse repetition interval, coherent and incoherent integrations can be selected to best adjust the eruption dynamics. More detail on VOLDORAD 2 is given in Donnadieu *et al.* (2003, 2005) and Dubosclard *et al.* (1999, 2004) describe similar processing of radar measurements made at Etna in 1998 with the radar prototype (VOLDORAD 1).

Following the processing of the series of Doppler spectra in the range gates located above the crater, time series can be computed for a set of positive (indexed +) and negative (indexed –) parameters, with the result of echoes from ejecta having a radial velocity component away from and towards the radar, respectively, corresponding mainly to respectively ascending and descending ballistics (Fig. 1). First, we define the power backscattered by particles with a radial velocity component away from (P^+) and towards (P^-) the radar within the considered range gate. The backscattered power is a complex function of the number and size of particles crossing the radar beam through their absorption and diffusion properties. Secondly, we define the mean velocity (V_{mean}^\pm) which corresponds to the average velocity of particles weighted by the power spectral density over the positive or negative velocity range. Then, we define the maximum radial velocity (V_{max}^\pm) of particles crossing the radar beam on both sides of the spectrum where the power spectral density becomes equal to the background noise level (Fig. 1). Finally, we define the spectral width of the Doppler spectrum from V_{max}^- to V_{max}^+ , which can be described as the variance of the spectral distribution. In the case where positive and negative parts of the Doppler spectrum are symmetrical and centred at 0 m s^{-1} , the spectral width can

be simplified to being twice the maximum positive radial velocity. This simplification is particularly useful here, where Strombolian explosions are very frequent (2–3 s). The consequence of this is that, during the paroxysm, the negative part of the Doppler spectrum in the range gate G_3 is always polluted by falling particles related to the previous explosion which combine with the echo signal of ascending particles having a motion component towards the radar antenna. This effect would hence bias any attempt to characterize initial jet properties (ascending particles only) by means of the total variance of the spectral distribution.

2.2 VOLDORAD recordings at Etna's SE Crater

From 2001 May to August, there were eruptions in the southeast crater every 3–5 d, each lasting on average a few hours and showing strombolian activity and lava fountain episodes. The radar soundings reported here were carried out over about 5 hr during the July 4 eruption (Donnadieu *et al.* 2003). The activity began at about 1800 UT, with small explosions recurring every 10 s on average. The intensity increased progressively, culminating in very powerful Strombolian explosions every 2–3 s, accompanied by the bursting of very large bubbles, between 2050 UT and 2145 UT. The eruption intensity then decreased rapidly from 2145 UT and activity ended around 2300 UT after a weak resumption around 2230. VOLDORAD was set up at an altitude of 3000 m, at a distance of about 1000 m to the crater rim, 280 m below and to the SSW of the summit of the SE crater, and with an antenna elevation angle of 23° (Fig. 2). The range gate G_3 was located right above the crater, centred at 1047 m from the antenna, and hence recorded the strongest echo power backscattered from particles. The vertical and radial resolution of G_3 was 165 and 120 m, respectively. The number of coherent integrations used for the Doppler spectra calculation determined a velocity range and resolution of 58.9 and 1.8 m s^{-1} , respectively, and an acquisition rate of about 8 Hz. Fig. 2 shows the geometric characteristics of the sounding at Etna's SE Crater during the

eruption of 2001 July 4, with the position of the radar range gates G_1 to G_4 , and the nomenclature of ejection angles as used in our analysis.

3 SYNTHETIC VOLCANO DOPPLER SPECTRA

Interpretation of Doppler spectra from Strombolian volcanic jets is made challenging by the wide range of particle sizes, ranging from millimetre-ash to metre-size blocks, as well as the variety of PSD. Indeed, the decoupling of ash-sized particles entrained by expanding gases from larger blocks following ballistic trajectories leads to a wide range of ejecta speeds, and to a large range of backscattered power spanning several orders of magnitude, hence its usual expression in dB (Log_{10}) scale. Also, the geometry of the jet, characterized by one EAD at each instant, strongly controls the shape of the Doppler spectra and it varies widely from one explosion to another. A thorough inspection of recorded Doppler spectra is not, alone, sufficient to place constraints on the dynamics of the Strombolian jets. To aid interpretation we have developed a complete model that generates synthetic Doppler spectra under controlled geometric and particle size conditions. In order to simulate synthetic Doppler spectra, we estimate the kinetic parameters from a ballistic model (Dubosclard *et al.* 2004), in particular, the radial velocity values for the x -axis of the Doppler spectrum, and we calculate the backscattered power needed for the y -axis of the Doppler spectrum from an electromagnetic model (Gouhier and Donnadieu 2008). More information on Doppler spectra modelling through the integration of both models can be found in the Appendix.

3.1 Estimation of kinetic parameters

To simulate the ejection of pyroclasts during a Strombolian explosion, we use the 2-D ballistic model developed by Dubosclard *et al.* (2004). Kinetic features are calculated based on the equations of

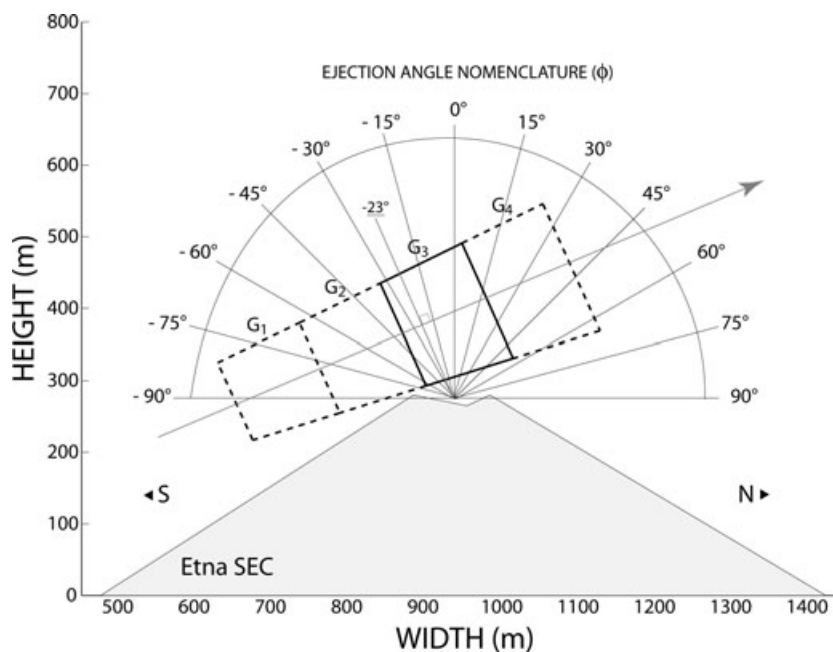


Figure 2. Radar sounding geometry at Etna's SE crater during the eruption of 2001 July 4, showing the location of four range gates (G_1 to G_4) from SSW to NNE. In this study, we focus on gate G_3 , positioned right above the crater. Ejection angles are indicated by ϕ with the vertical axis taken as 0° . Elevation scale on the left is relative to the radar altitude (~ 3000 m a.s.l.).

motion, assuming that the two forces acting on each particle are drag and gravity. The initial velocity of a particle with diameter D is defined on input into the model as (Steinberg & Babenko 1978)

$$V_0^p(D) = V_0^g - k\sqrt{D}, \quad (1)$$

where V_0^g is the initial gas velocity and k is an empirical constant taken as 150, as inferred from previous studies (Chouet *et al.* 1974; Ripepe *et al.* 1993). The gas velocity decreases exponentially with height as follows:

$$V_g(z) = V_0^g \exp(-\gamma z). \quad (2)$$

The gas velocity decay rate is a major unknown, being very difficult to measure accurately in the field. Here we use a decay value $\gamma = 0.013$ inferred from the best fit of height vs. velocity measurements carried out at Stromboli on 39 explosions by Patrick *et al.* (2007). This value has been inferred from ash-rich Strombolian eruptions, with gas velocities $<50 \text{ m s}^{-1}$, and may vary from one explosion type to another. Other measurements carried out by Blackburn *et al.* (1976) at Stromboli, provide a higher gas velocity decay rate ($\gamma = 0.022$), but this is based on only eight observations, and using a visible camera. The value inferred from Patrick *et al.* (2007) was acquired using a Forward Looking Infrared Radiometer (FLIR) camera, which enables a better distinction of the gas phase from particles and the precise tracking of the gas expansion from the crater rim up to 150 m in height in this case. Furthermore, tests carried out to assess the sensitivity of particle velocity using both gas velocity decay values show no significant effect for the particle size used here (around 0.1 m), with a difference of only 1 per cent in velocity at the height of the radar sampling volume.

We have modelled in Fig. 3 a test explosion with a uniform polydisperse PSD ranging from 0.01 to 0.1 m, and with a Gaussian distribution of ejection angles (EAD) ranging from -45° to $+45^\circ$,

centred on the vertical axis. We use 4520 spherical particles propelled upwards using an initial gas velocity $V_0^g = 100 \text{ m s}^{-1}$. In our simulation, the location of the vent was taken to be 50 m beneath the crater rim because it was observed to be 66 m deep after the eruption on July 7 (Patrick Allard, personal communication, 2009) but was partially filled with lava at the time of the eruption paroxysm.

The radial velocity of each particle is calculated from the ballistic model with a 0.01 s time step. The temporal evolution of the mean and maximum radial velocities are then plotted (Fig. 4) for the range gates G_3 and G_4 , located at 1047 and 1167 m from the radar, respectively. Importantly, the mean radial velocity calculated by the model represents the arithmetic average of the along-beam (radial) velocity components of all particles in the range gate, not the power-weighted mean radial velocity, as measured from the radar data, whose physical meaning is more complex. The maximum radial velocity corresponds to the largest particle velocity calculated along-beam (radial).

The patterns of mean and maximum velocities in range gate G_4 are quite similar, whereas they differ significantly in range gate G_3 , located right above the vent. These differences come from the radar sounding geometry. The radial component of velocity (i.e. along-beam, as measured by the radar) becomes lower as particle trajectories depart from the beam axis, and ultimately reaches zero when the particle trajectory is perpendicular to the beam ($\sim 90^\circ + 23^\circ$). Most particles in the range gate G_3 have a trajectory with a strong vertical component; therefore the mean radial velocity of particles in G_3 ($t = 1 \text{ s}$; $V_{\text{mean}} = 26 \text{ m s}^{-1}$) largely underestimates the real mean velocity at this instant (Fig. 4a). On the contrary, more particle trajectories become tangential to the beam in range gate G_4 as ballistic particles deviate from their initial trajectory during the ballistic flight, so the mean radial velocity of particles in G_4 ($t = 1.5 \text{ s}$; $V_{\text{mean}} = 50 \text{ m s}^{-1}$) gives a better estimate of the real mean velocity. Note, however, that velocities of particles inside

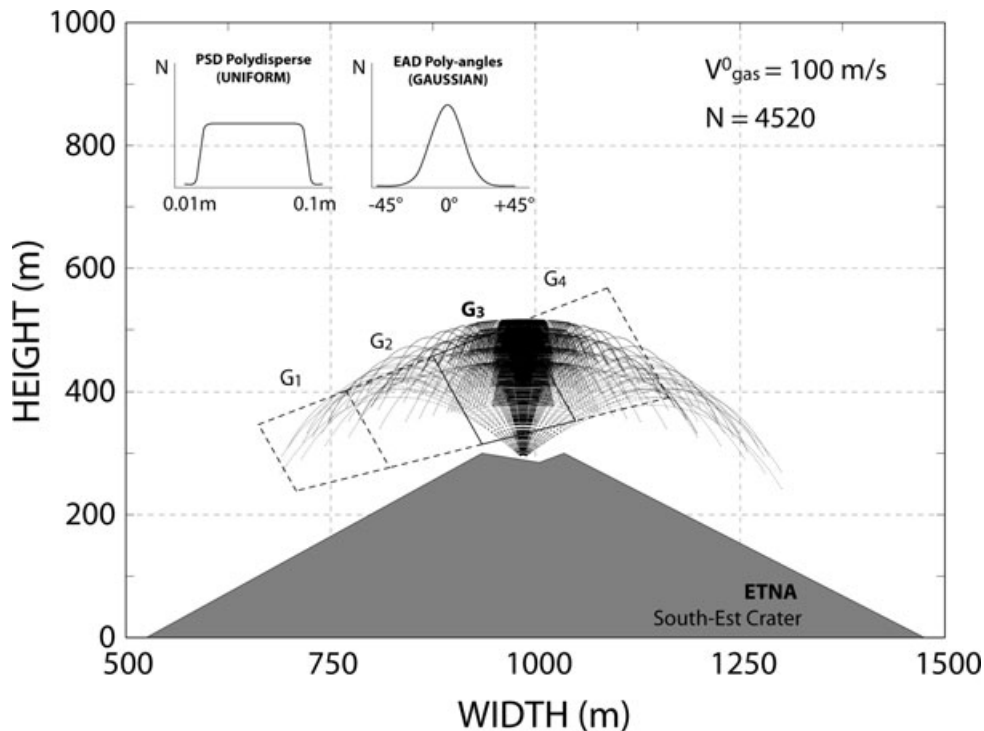


Figure 3. Ejecta trajectories calculated from the ballistic model for a test explosion with 4520 particles. Inputs are shown as inserts: uniform particle size distribution (PSD) ranging from 0.01 to 0.1 m, Gaussian ejection angle distribution (EAD), ranging from -45° to $+45^\circ$, initial gas velocity of 100 m s^{-1} .

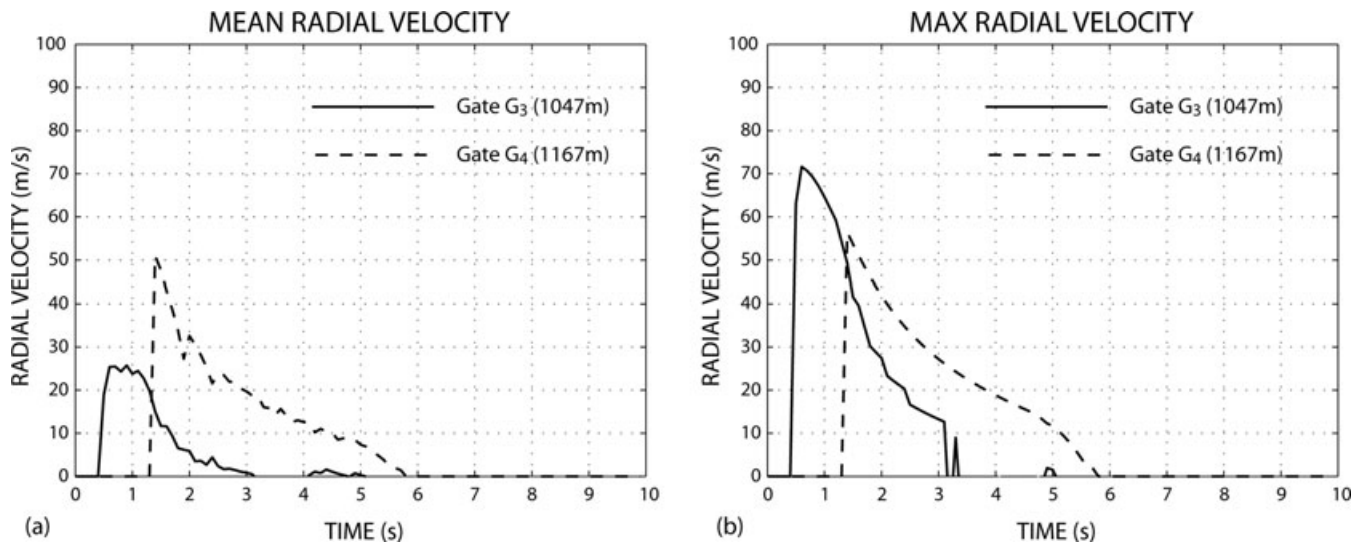


Figure 4. Time-series of velocities inferred from the ballistic model for the test explosion in range gates G_3 and G_4 : (a) mean radial velocity, representing the arithmetic average of the along-beam velocity components of all particles in the range gate and (b) maximum radial velocity calculated.

gate G_4 have already slowed down because of the large distance covered from the point of emission (~ 120 m) and therefore do not represent initial (at-vent) values. The maximum value of the radial velocity in gate G_3 ($t = 0.6$ s; $V_{\max} = 71$ m s $^{-1}$) is higher than that reached in gate G_4 (56 m s $^{-1}$), but is still underestimated for the reasons already outlined above (Fig. 4b). At the onset of the time-series, the maximum radial velocity corresponds to the finest particles which closely follow the gas motion, and show a strong decrease in speed. Progressively, after a few seconds, larger particles with high inertia become faster than these small ones, as the larger particles have a lower velocity decrease. The results of this section show that meaningful synthetic velocities can be derived from the ballistic model for a wide range of particle sizes at each time step in every range gate. In the next section we derive, under the same conditions, the synthetic power backscattered by particles from the electromagnetic model developed by Gouhier & Donnadieu (2008).

3.2 Estimation of backscattered power

The power backscattered by spherical particles is derived from the electromagnetic wave scattering theory of Mie (1908), using the complete set of equations applied to our specific case given in Gouhier & Donnadieu (2008). A good approximation can be obtained, with reduced computing time, by applying the Rayleigh analytical solution, but this is only applicable for particles with a diameter of less than $\lambda/4$, that is, ~ 5.9 cm in our case (Gouhier & Donnadieu 2006). Given the wide range of particle diameters characterizing Strombolian activity, the Mie scattering theory is required to account for the effects of larger particles. Full development of the electromagnetic model can be found in Gouhier & Donnadieu (2008). Note that our model also takes into account the power distribution intensity across with the beam using a Gaussian function, as defined for instance in Sauvageot (1992).

The power backscattered by each particle is calculated from the electromagnetic scattering model at each time step. Fig. 5 shows the temporal evolution of synthetic power in the radar range gates G_3 and G_4 . The synthetic echo power signal in G_3 gives higher values, and is shorter than in G_4 . Both features can be explained by the fact that the majority of emitted particles cross the gate directly above the vent (G_3), whereas only a fraction enter the next range

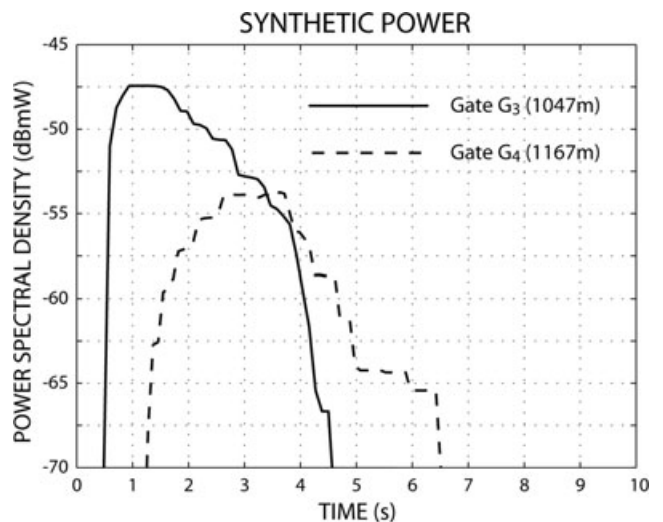


Figure 5. Time-series of the synthetic power backscattered by particles in range gates G_3 and G_4 calculated from the electromagnetic scattering model at each time step, for the test explosion shown in Fig. 3.

gate (G_4) with the delay time necessary for particles to cross G_3 . Moreover, their velocities have significantly decreased and their trajectories become more slanting, so the residence time in G_4 is longer. Synthetic values of power and velocities calculated from these combined models are used first to construct synthetic Doppler spectra, and are then subsequently compared to the Doppler spectra measured by VOLDORAD.

3.3 Synthetic Doppler spectra

Synthetic Doppler spectra can be constructed using both radial velocities and backscattered power values derived from the ballistic and electromagnetic scattering models, respectively. They are calculated every 0.1 s so as to correspond to the acquisition rate (~ 10 Hz) of the recorded Doppler spectra in each range gate. The synthetic Doppler spectra are built up by dividing calculated particle velocities into classes and then summing the power backscattered by the corresponding particles for each velocity class. The

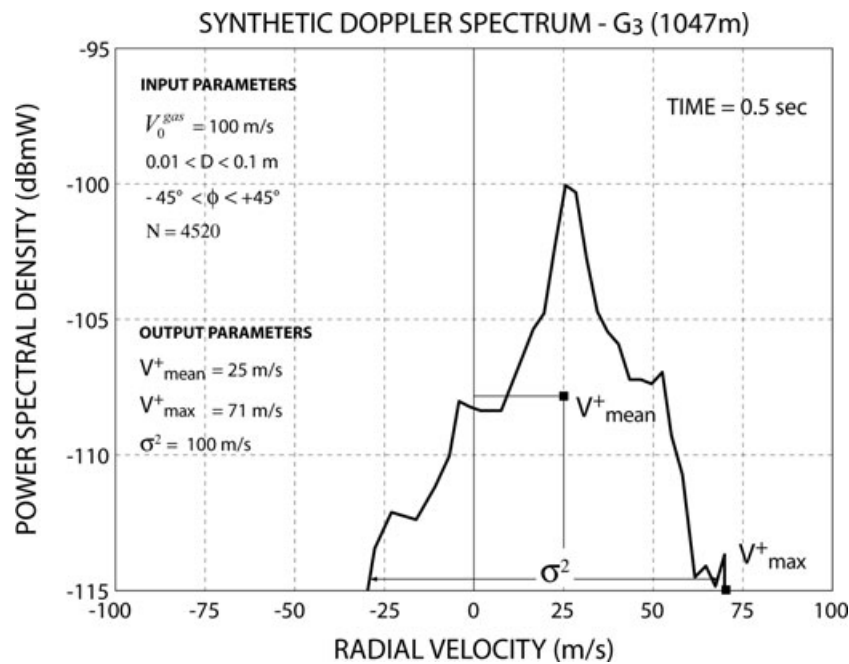


Figure 6. Synthetic Doppler spectrum of the test explosion modelled from the ballistic and electromagnetic scattering models showing the power spectral density as a function of radial velocities. Spectral moments (spectral width, maximum and mean velocities) are calculated from the spectrum in the same way as VOLDORAD.

velocity range and classes can be adapted according to the conditions of the modelled explosion. The distribution of the backscattered power over the velocity range defines the power spectral density, expressed in dBmW (mW in Log_{10} scale). Fig. 6 shows the synthetic Doppler spectrum in range gate G_3 , 0.5 s after the onset of the explosion. In this specific case, the velocity range is $\pm 100 \text{ m s}^{-1}$, divided into 40 velocity classes, hence a velocity resolution of 5 m s^{-1} .

We observe that the synthetic Doppler spectrum is quite triangular, roughly symmetric, and centred on the positive part. In this case, the mode corresponds to the mean radial velocity of $\sim 25 \text{ m s}^{-1}$. The synthetic maximum radial velocities obtained are 71 and -29 m s^{-1} for the positive and negative part, respectively, giving a spectral width of $\sim 100 \text{ m s}^{-1}$. Note that there is no noise level in modelled Doppler spectra, so the maximum velocity of each individual particle, even small ones, can be computed. We point out that the maximum positive radial velocity obtained from the synthetic Doppler spectrum (i.e. in the same way as VOLDORAD) equals the peak of maximum particle velocity observed in the time-series (Fig. 4b). This result emphasizes that maximum velocities are not biased by the power distribution in our radar model. This first model demonstrates the effectiveness of this method for modelling synthetic Doppler spectra, and emphasizes the strength of this approach for the characterization of geometric features. Following this, we aim to reproduce real volcanic Doppler spectra, and fit the shape of recorded Doppler spectra in order to derive dynamic parameters. It must be noted that we do not aim to match the actual, measured power in our model because it would be useless for our purpose and computationally time-consuming since the number of particles in the model would have to be increased. Quantitative measurements of geometric parameters are not affected by this simplification since they can be retrieved directly from the spectrum shape. The model inputs required are the PSD, the EAD and the initial gas velocity. We retrieve as an output the mean and maximum radial velocities as well as the spectral width, which partially

define the shape of a Doppler spectrum. Later we explore in more detail the effects on the shape of the spectrum (see Section 4.2). The match between the synthetic and recorded Doppler spectra is achieved using trial-and-error tests in order to best take into account all the characteristics of recorded Doppler spectra.

4 PARAMETRIC TESTS

Any volcanic Doppler spectrum is potentially a valuable source of information of the explosion dynamics. The study of the Doppler spectrum shape, in particular, can constrain the geometry of the particle ejection. The shape of a Doppler spectrum, which represents the distribution of backscattered power as a function of the radial velocity, may be influenced by numerous factors. Some factors may play a role in the power of the spectrum (y -axis), such as the number and size of ejected particles, and, to a lesser degree, particle properties (composition, shape and temperature). Other factors may control the radial velocity of the spectrum (x -axis), such as the particle velocity controlled by the gas velocity and particle size, the particle ejection angle determining the value of the along-beam component of velocity measured by the radar, and the turbulence in the plume. Some of these factors are constant, such as particle properties, as well as geometric features of the sounding (size of the range gate, beam elevation, etc.), and do not control the variability of the Doppler spectrum shape. The effect of turbulence in the cloud is difficult to assess; from a radar perspective, however, the backscattered power is strongly controlled by large blocks mostly following ballistic trajectories, so we assume that this effect is small. If it exists, the effect of turbulence would be to increase the spectral width (σ^2), as observed in radar meteorology. The variation of the initial gas velocity would affect the range of particle radial velocities, but no significant variation in the shape of the Doppler spectra is expected.

Henceforth, we identify two main factors as variables which significantly influence the spectral patterns: (1) the EAD, which

strongly influences the measured radial velocities and (2) the PSD which accounts for both the variability of ejecta speeds and the power backscattered. In the following, we carry out simple parametric tests to assess the contribution of both these potential biases in the retrieval of quantitative parameters from volcanic Doppler spectra. Note that tests on the effect of wind have not been carried out as it was relatively calm on 2001 July 4. Acoustic measurements by Vergniolle & Ripepe (2008) measured wind speeds in the range of 4–6 m s⁻¹.

4.1 Model sensitivity to EAD and PSD

Fig. 7(a) shows a synthetic Doppler spectrum with a single peak at 23 m s⁻¹ resulting from the simplistic case of a single particle of diameter $D = 0.03$ m (monodisperse PSD) launched vertically at $\phi = 0^\circ$ (mono-angle EAD), with an initial gas velocity of 100 m s⁻¹. In Fig. 7(b), a narrow Doppler spectrum (spectral width < 10 m s⁻¹) is modelled with all particles ejected also vertically (mono-angle EAD), but using an even spread PSD with diameters ranging from 0.003 to 0.06 m (polydisperse PSD). By comparison

with the previous case, one can see that a wide PSD alone does not account for the large dispersion of radial velocities observed in volcanic Doppler spectra, even if additional larger blocks were considered. In contrast, we modelled in Fig. 7(c) an explosion with single-sized particles (monodisperse PSD, $D = 0.03$ m), launched at various angles ranging uniformly from -45° to $+45^\circ$ to the vertical (poly-angle EAD). We observe in this case a top-hat Doppler spectrum with a large spectral width of about 85 m s⁻¹. This clearly emphasizes the overall influence of jet collimation on the range of measured radial velocities. A more realistic simulation is shown in Fig. 7(d), where particles were launched over an even spread of EAD (-45° to $+45^\circ$), and an even spread of PSD (0.003–0.6 m). The resulting Doppler spectrum is slightly larger than the one in Fig. 7(c) because of the existence of very fine particles (0.003 m) following the gas motion, and hence having higher velocities. Also, the power spectral density is a little higher, due to the existence of larger particles (0.06 m) backscattering much more power. However, despite differences between Figs 7(c) and (d) related to the use of a polydisperse PSD, one can observe that the overall shape is quite similar, as the same EAD is used in both cases. In addition,

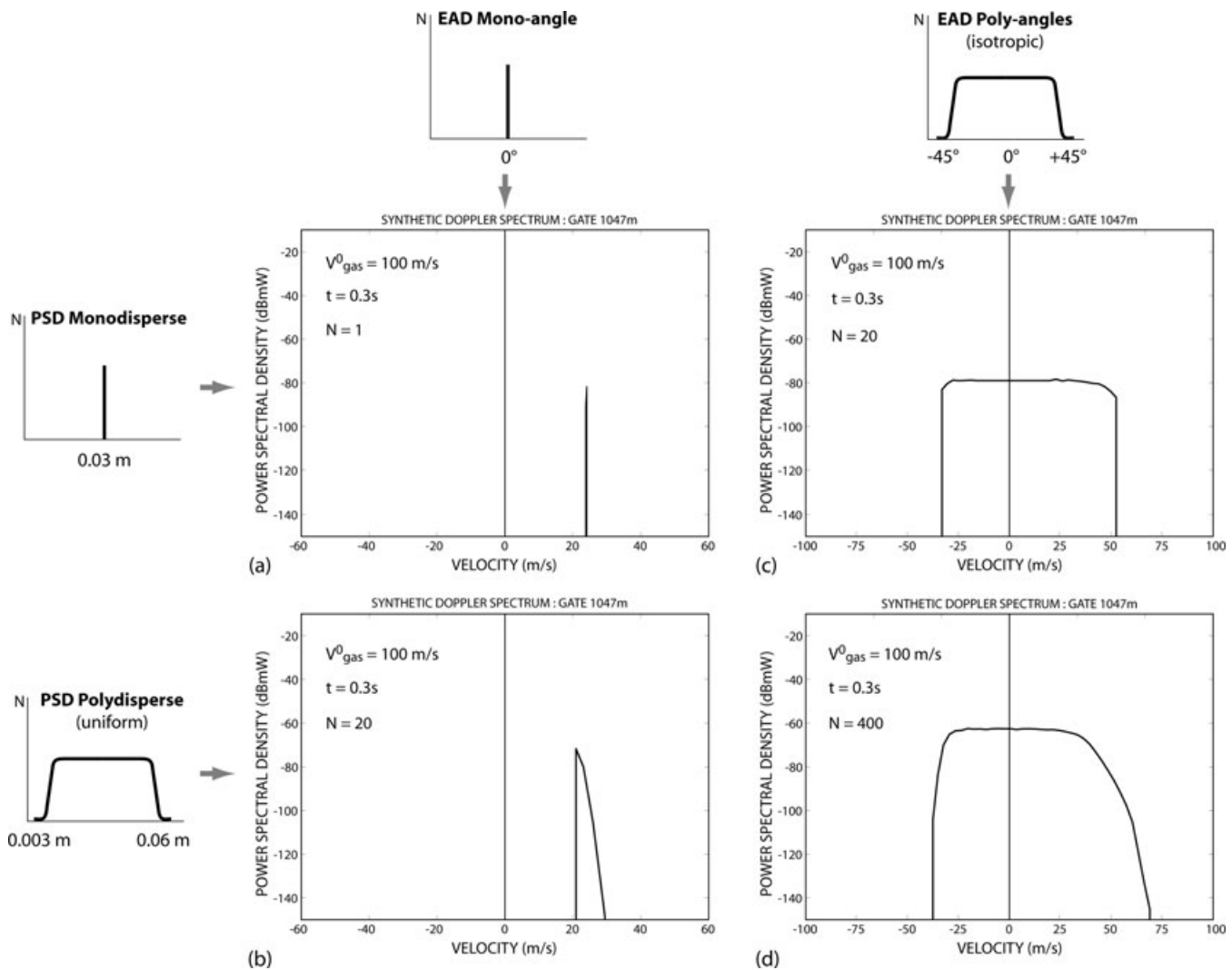


Figure 7. Synthetic Doppler spectra showing the contribution of ejection angle distributions (EAD – upper inserts) and particle size distributions (PSD – left inserts) on the shape variability of volcanic Doppler spectra. (a) Vertical ejection ($\phi = 0^\circ$) of single diameter particles ($D = 0.03$ m). (b) Vertical ejection ($\phi = 0^\circ$) with uniform PSD ($0.003 \text{ m} < D < 0.06 \text{ m}$). (c) Uniform EAD ($-45^\circ < \phi < +45^\circ$) of single diameter particles ($D = 0.03$ m). (d) Uniform EAD ($-45^\circ < \phi < +45^\circ$) with uniform PSD ($0.003 \text{ m} < D < 0.06 \text{ m}$).

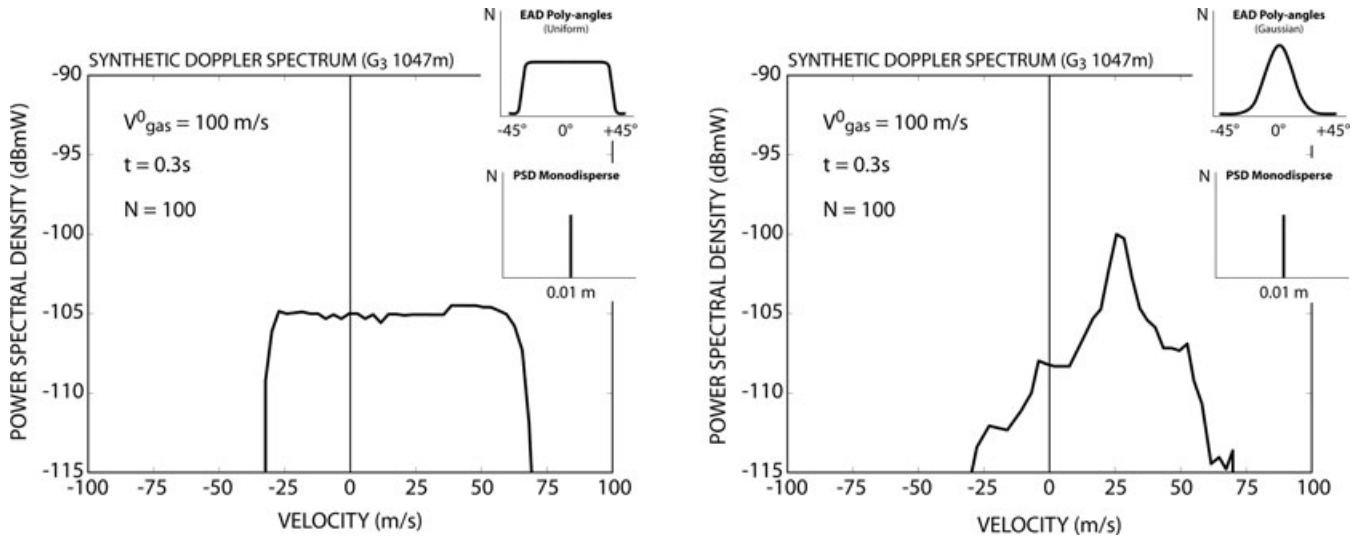


Figure 8. (a) Top-hat-shaped Doppler spectrum induced by a uniform EAD; (b) triangular-shaped Doppler spectrum induced by a Gaussian EAD. Model inputs and results are indicated in the figures and inserts; PSD is monodisperse with $D = 0.01$ m (bottom inserts).

in reality these Doppler spectra (Figs 7c and d) would look even more alike because of the noise of the radar system. These simple characteristic tests point out that the dominant effect on the spectra shape clearly stems from the geometrical distribution of particle ejection angles.

4.2 Influence of the EAD

We have carried out many other parametric tests in order to refine our interpretations of radar Doppler spectra. We do not aim, however, to present them all exhaustively, but instead to sum up the main characteristics that might control the shape of the Doppler spectra. We have shown previously the dominant role played by the particle ejection geometry and, to a lesser extent, by the range of particle sizes. However, all the explosions modelled so far have had uniform EADs. We now investigate how sensitive the shape of a Doppler spectrum is to the variability of the EAD. In Fig. 8 two explosions are modelled with different poly-angle EADs and a fixed monodisperse PSD with a diameter $D = 0.01$ m. For each explosion tested, the maximum radial velocities as well as the spectral widths are found to be the same, but two main shapes can be distinguished: top-hat and triangular Doppler spectra. Similar observations have already been made by Hort *et al.* (2003). The first explosion modelled (Fig. 8a) follows a uniform EAD, with ejection angles ranging from -45° to $+45^\circ$. It means that the same amount of volcanic material is ejected in all directions. This feature can be directly interpreted from the top-hat shape of the Doppler spectrum with the plateau part having the same power amplitude over the velocity range -28 to $+72$ m s^{-1} . Henceforth, we make the distinction between the plateau spectral width (σ_p^2), indicating uniform ejection, and the total spectral width (σ^2), where the slopes of the top-hat Doppler spectrum are subvertical; in this particular case $\sigma_p^2 - \sigma^2 = 100$ m s^{-1} .

In a contrasting case, the second explosion (Fig. 8b) follows a Gaussian EAD, with angles ranging from -45° to $+45^\circ$. This means that the amount of particles dramatically decreases at high ejection angles, that is, away from the vertical. This feature is clearly seen from the triangular shape of the Doppler spectrum and the marked decrease of power on either side of the power peak. Since there is no plateau component only the total spectral width can be determined,

which in this case is the same as for the previous explosion modelled ($\sigma^2 = 100$ m s^{-1}).

4.3 Jet axis inclination

Lastly we carried out some parametric tests to assess the sensitivity of the Doppler spectrum shape to the jet inclination. Fig. 9 shows four spectra modelled using an initially Gaussian EAD inclined at 20° , 0° , -20° and -40° to the vertical. Note that all Doppler spectra are triangular, as would be expected from a Gaussian EAD. Doppler spectra are modelled using particles with a single diameter of 0.01 m and an initial gas velocity of 100 m s^{-1} . Interestingly, the mode of the Doppler spectra, that is, the radial velocity associated with the maximum of the power spectral density, provides information on the jet orientation. This radial velocity can be regarded as the velocity projection onto the beam axis of the ejection direction bearing the largest load of ejecta, that is, the jet axis. Although the jet axis cannot be fully recovered in 3-D from the spectrum mode alone, its inclination can be constrained in the vertical plane containing the emission source and the beam axis. In these examples, the power mode values fall, respectively, at about 50 , 25 , 0 and -25 m s^{-1} for the four EAD chosen. Remarkably, a vertically oriented jet induces a power mode at a radial velocity $V_\phi = 0 = +25$ m s^{-1} under the initial conditions chosen previously (Fig. 8b). Consequently, jets inclined away from the radar ($\phi > 0^\circ$), generate a power mode which exceeds this radial velocity threshold, whereas jets inclined toward the radar ($\phi < 0^\circ$) generate a power mode of less than $V_\phi = 0$. Note that the power mode is 0 m s^{-1} when the main jet orientation is perpendicular to the beam axis (Fig. 8c). Depending on the position of the particles inside the gate, this angle may vary from -18.5° (bottom of G_3) to 27.5° (top of G_3). Thus, based on the reasonable assumption that there is a weak influence of the PSD on the shape of the Doppler spectrum, the jet inclination in a vertical plane passing through the beam can be readily obtained using the power mode, given an initial gas velocity and the sounding geometry.

Parametric tests described in this section highlight the potential information contained in Doppler spectra for understanding the kinematics of volcanic jets, and particularly for estimating jet orientations. We show in the following sections that some of these

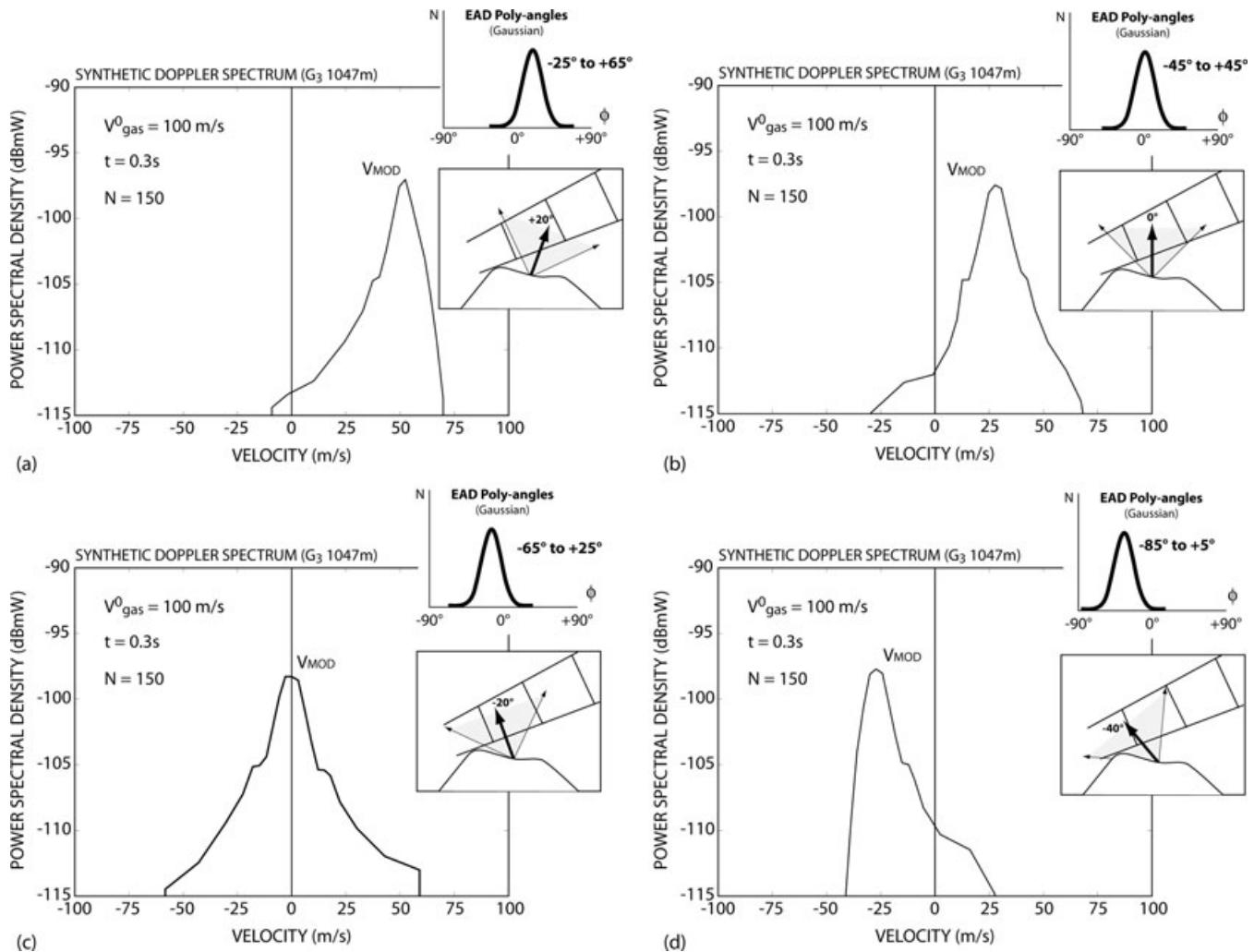


Figure 9. Sensitivity of the mode of the power spectral density to the jet inclination in synthetic Doppler spectra of strombolian explosions. Single sized particles ($D = 0.01$ m) are propelled at various angles (poly-angle EADs, upper insert) following a Gaussian distribution. The mode of the angle distribution, i.e. the main initial ejection direction, has values of (a) $+20^\circ$, (b) 0° , (c) -20° and (d) -40° relative to the vertical (lower inserts).

individual characteristics can be applied to the Doppler spectra recorded by VOLDORAD at Mt Etna, in order to retrieve geometrical parameters characterizing Strombolian explosions.

5 CASE STUDY: GEOMETRICAL PROPERTIES OF TWO CONTRASTING STROMBOLIAN EXPLOSIONS

In this section, we characterize the geometrical aspects of Strombolian explosions produced by Mt Etna SEC. Typical Strombolian activity consists of a series of large bubbles rising from depth through the magmatic conduit, and disrupting the overlying magmatic film when they reach the surface (e.g. Vergnolle & Brandeis 1996). The bubble overpressure release is then responsible for the ejection of a range of particle sizes from fine particles to large disconnected blocks above the vent, which then cross the radar beam. The dynamics of Strombolian explosions are complex, and the study of the geometrical characteristics of such volcanic jets aims to place constraints on the physical source mechanisms at work. The analysis of Doppler spectra recorded by VOLDORAD shows the existence of two main shapes: top-hat and triangular. We focus here on two particular explosions with contrasted geometrical features that oc-

curred on 2001 July 4, and propose a method to retrieve source parameters from the modelling of both spectrum shapes.

5.1 Top-hat-shaped spectra

In Fig. 10, we have reproduced a Strombolian explosion that occurred on 2001 July 4, at 21:43:04 UT during the paroxysm of the eruptive episode. In this example, the overall shape of the recorded Doppler spectrum is typically top-hat (Figs 10a and c), displaying two distinct parts: (1) a broad plateau characterized by a spectral width of $\sigma_p^2 = 35 \text{ m s}^{-1}$, bordered by (2) steep slopes reaching a noise level at about $V_{\text{max}}^+ = 40 \text{ m s}^{-1}$ on the positive scale. The corresponding video snapshot shows the rather hemispheric ejection of large lava clots following the free bubble expansion and outburst. This suggests a rather uniform ejection of particles moving radially from the vent and ejected with seemingly relatively homogeneous velocities. Note that this kind of event is not the most common, occurring mainly during the paroxysmal phase when the magma level in the conduit is high and partially fills the crater.

Previous photoballistic studies at Etna have shown that for one Strombolian explosion of the northeast Crater, in 1969 June, 50 per cent of the ejecta were between 0.1 and 0.4 m in size (McGetchin

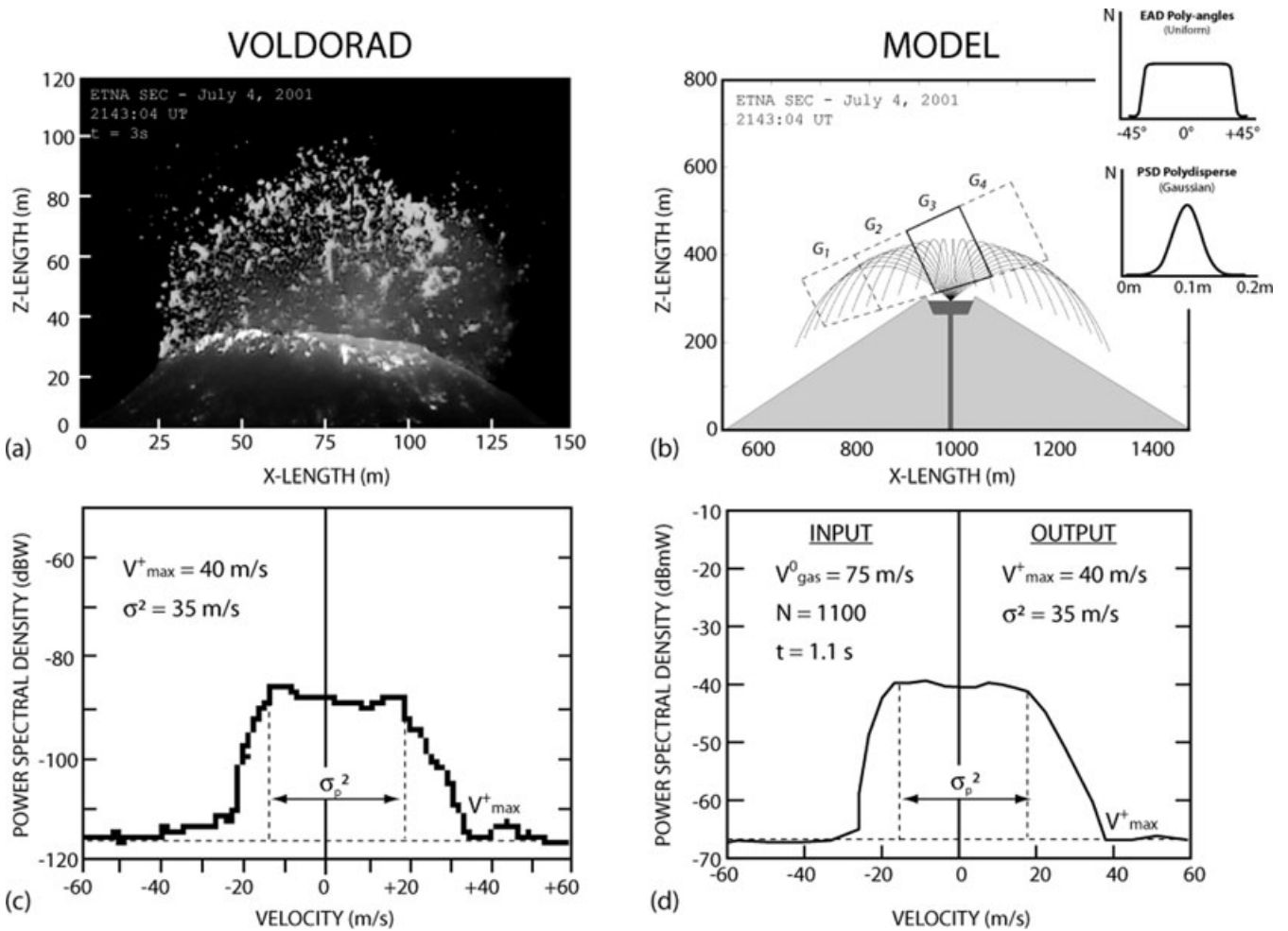


Figure 10. (a) Video snapshot of a lava bubble outburst occurring at Etna’s SE Crater, at 21:43’04 UT on 2001 July 4. (b) Visual representation of this explosion with the ballistic model. (c) VOLDORAD Doppler spectrum with top-hat shape; ground-echoes have been removed. (d) Synthetic Doppler spectra obtained with indicated input parameters.

et al. 1974). Ground deposit studies have also calculated similar sizes of scoria blocks produced by Strombolian activity at Etna on 2001 July 25–31 (Métrich *et al.* 2004). Modelling of acoustic waves at Etna has provided a characteristic thickness of the magmatic film overlying the gas bubble right before its rupture, assumed to be on the order of the average size of the blocks formed thereafter, of about 0.1 m (Vergniolle & Ripepe 2008). These constraints on the particle sizes at Etna led us to run our model on this explosion with a polydisperse Gaussian PSD centred at 0.1 m. A synthetic top-hat shaped Doppler spectrum (Fig. 10d) has successfully been modelled from the simulation of a Strombolian explosion having a uniform EAD with angles ranging from -45° to 45° , and an initial gas velocity of $V_0^g = 75 \text{ m s}^{-1}$. This result confirms that the top-hat Doppler spectrum is therefore typically representative of a uniform distribution of nearly all ejecta emitted radially from the source vent. The synthetic plateau spectral width and maximum radial velocity are very close to those measured by VOLDORAD, and the slopes are also very steep.

5.2 Triangular-shaped spectra

We have also modelled a contrasting style of explosion, typical of a dense vertically oriented Strombolian jet, such as the explosion

that occurred at 21:39:34 UT on 2001 July 4 (Fig. 11). The bubble expansion could not be seen on the video recording, suggesting that the bubble burst below the level of the crater rim, and hence was partially constrained laterally by the crater or conduit walls.

The video analysis reveals that the main jet orientation is close to vertical, with a higher concentration of particles in the inner core, as indicated by the higher intensity of light scattered (Fig. 11a). Although we are aware that the mean ejecta size may vary, here we have kept a Gaussian PSD centred at 0.1 m as an input to the model, as assumed for the previous case. Using trial-and-error tests, a synthetic triangular-shaped Doppler spectrum (Fig. 11d) has again been modelled successfully, with a Gaussian EAD using angles ranging from -40° to 40° , and with an initial gas velocity of $V_0^g = 125 \text{ m s}^{-1}$. Although this model solution is not unique, this result strongly argues that triangular Doppler spectra are representative of a Gaussian distribution of ejecta with a maximum concentration in the jet axis, that is, in this case vertically above the source ($\phi = 0$), and decreasing sideways. Geometrically, the triangular-shaped Doppler spectra comprise two non-vertical slopes with a single power maximum. The synthetic spectral width and the maximum radial velocity are found to be the same as those measured by VOLDORAD, with values reaching 90 and 60 m s^{-1} , respectively. The mode, that is, the radial velocity corresponding to the power peak, is also in agreement with the one measured on the recorded

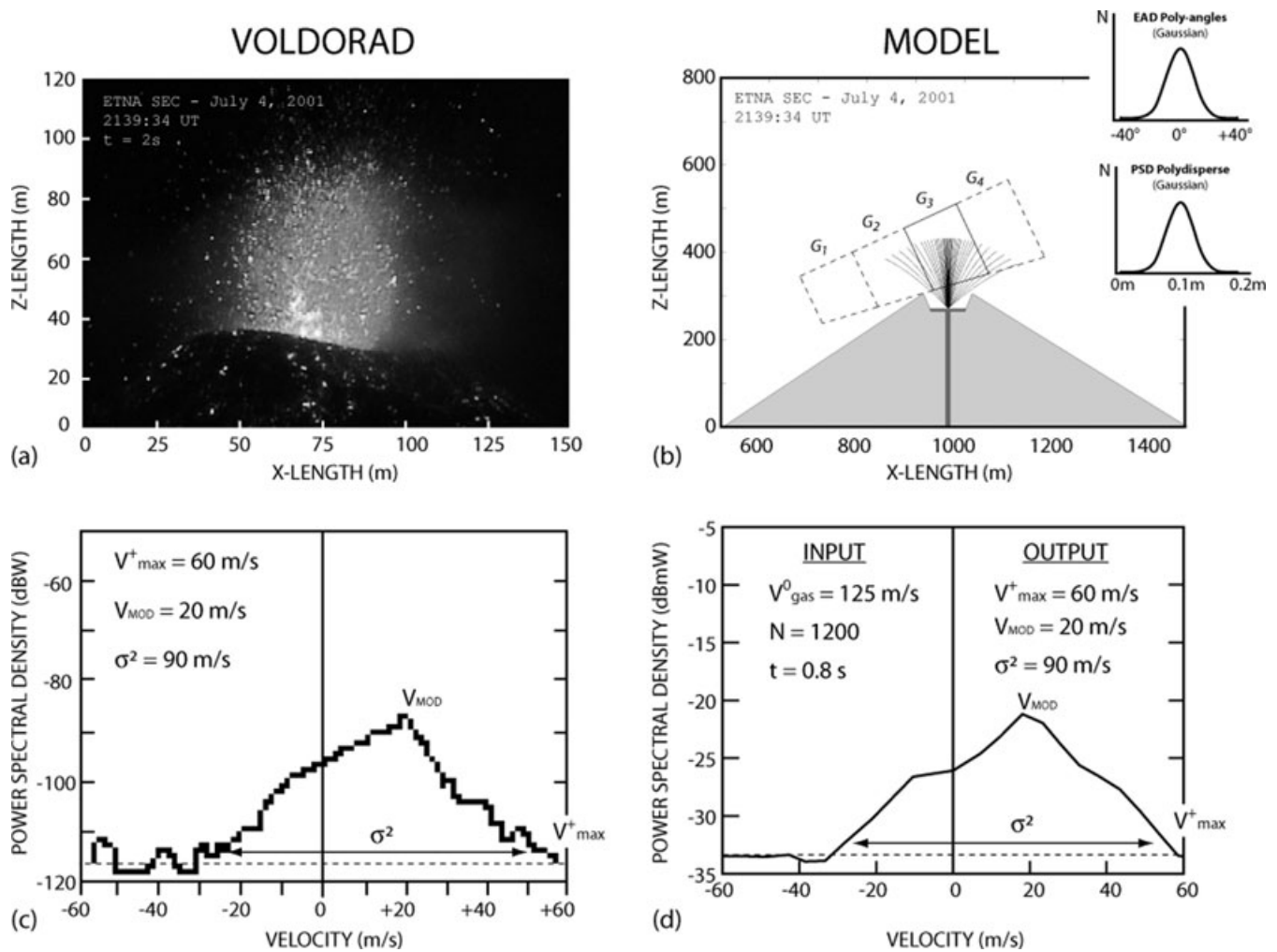


Figure 11. (a) Video snapshot of a Strombolian lava jet occurring at Etna's SE Crater, at 2139:34 UT on 2001 July 4. (b) Visual representation of this explosion with the ballistic model. (c) VOLDORAD Doppler spectrum with triangular shape; ground-echoes have been removed. (d) Synthetic Doppler spectrum obtained with indicated input parameters.

spectrum (20 m s^{-1}), showing that the main orientation of the jet is subvertical. We have calculated from the echo power ratio that about 80 per cent of the total amount of particles are ejected within a dispersion cone 40° wide centred on the vertical axis (-20° to 20°). This angle has been directly deduced from the relation between radial velocity and cone aperture at the initial gas velocity of 125 m s^{-1} and a particle size of 0.1 m . The remaining 20 per cent is distributed between this inner cone and the limit of the range of ejection angles (from -40° to -20° and from $+40^\circ$ to $+20^\circ$). The marked depletion of particles around the sides of the jet, that is, at higher ejection angles, explains the slanted slope of the triangular Doppler spectrum.

6 STATISTICAL ANALYSES OF GEOMETRICAL FEATURES

The detailed analysis of two specific Strombolian explosions has pointed out the close relationships between the shape of Doppler spectra and the geometry of the volcanic jet. In this section, we give quantitative estimates of geometric parameters for more than 200 Strombolian explosions.

6.1 Relationship between radial velocity and ejection angle

In order to provide statistical results on a large number of events relatively quickly, we defined a monodisperse PSD ($D = 0.1 \text{ m}$) and a constant value of the initial gas velocity ($V_0^g = 150$) for all explosions studied. The validity limit of this approach is clearly directly linked to these assumptions, because the gas velocity varies significantly from one explosion to another. Therefore, we carried out additional calculations (Fig. 12) to show the influence of these two assumptions on the relation between radial velocities and ejection angles. Fig. 12(a) shows the relationship between radial velocities and ejection angles for different values of initial gas velocities ranging from 100 to 250 m s^{-1} , and for a constant particle diameter of $D = 0.1 \text{ m}$. The variability between each curve is relatively marked, stressing the importance of the initial gas velocity chosen. Fig. 12(b) shows the relationship between radial velocities and ejection angles for various diameters extending over most of the natural range from 0.01 to 0.2 m , and for a constant initial gas velocity of 150 m s^{-1} . The variability is less in this case, and the choice of the reference diameter appears less critical, except at unaturally high ejection angles.

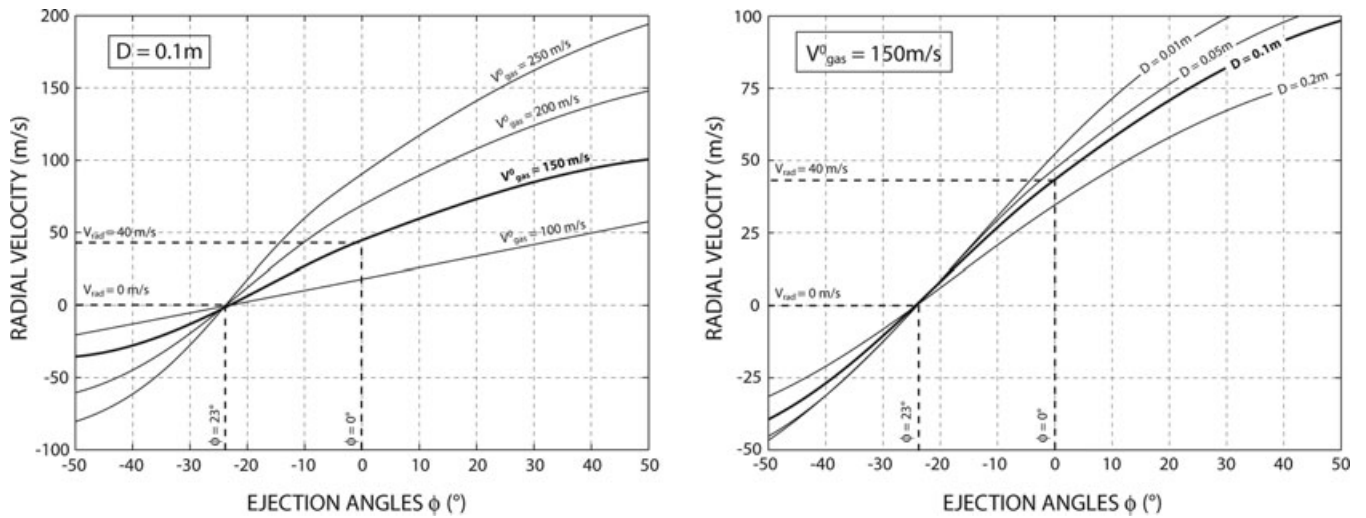


Figure 12. Abacuses showing the relationships between the radial velocity and the particle ejection angles for (a) variable initial gas velocities (constant diameter $D = 0.1$ m) and (b) variable diameters (constant initial gas velocity of 150 m s^{-1}).

The statistical analysis was carried out on about 200 explosions that took place between 21:00 U.T. and 21:45 U.T. during the paroxysmal phase of the eruption of 2001 July 4 at Etna’s SE Crater. The systematic analysis of Doppler spectra, once the ground echoes have been removed, shows that only 12 per cent of explosions have a typical top-hat-shaped spectrum, comprising a large plateau bordered by subvertical slopes. 34 per cent of the Strombolian events have a purely triangular-shaped spectrum (without plateau) characterized by a single power maximum. The majority (54 per cent) of the Strombolian explosions studied have a spectrum shape intermediate between both end-members described above, with a plateau bordered by non-vertical slopes.

6.2 Pyroclast dispersion cone with uniform distribution

Modelling of the explosion at 21:43’04 UT (Fig. 10) highlights the close relationship between the plateau spectral width and the aperture of the uniform ejection cone. Recall that σ_p^2 was defined as twice the maximum velocity in order to eliminate the power signal derived from falling particles. In this section we focus on the characterization of the uniformly distributed ejection cone. We thus take into account both pure top-hat and intermediate Doppler spectra, which we call hereafter plateau-type Doppler spectra. Together they represent 2/3 of all the Strombolian explosions studied.

Fig. 13(a) gives the proportion of plateau-type explosions for different classes of cone apertures for which the EAD is uniform. We find that most of these explosions present a uniform distribution of ejecta within a cone $\sim 40^\circ$ wide (i.e. -20° to $+20^\circ$), with a global distribution which is roughly log-normal. Note that particles are also present outside this cone, albeit at concentrations which decrease radially. We have carried out the same analysis for different initial gas velocities in order to show the potential error made by our first order estimations. We find a characteristic cone aperture of $\sim 90^\circ$ (i.e. -45° to 45°) and $\sim 30^\circ$ (i.e. -15° to 15°) for initial gas velocities of 100 and 200 m s^{-1} , respectively. However, the results we found using $V_0^g = 150 \text{ m s}^{-1}$ are consistent with deductions from the photoballistic study of one Strombolian explosion at Etna’s northeast Crater by McGetchin *et al.* (1974), who found that ejection angles were distributed uniformly within a dispersion cone 30° wide.

6.3 Relative ejecta concentration within the dispersion cone

In this section, we examine the relative particle concentrations inside the whole jet, taking into account all Doppler spectra, including both plateau-type and triangular-type. We again note that the power backscattered to the radar is related to the number (N) and size (D) of particles crossing the antenna beam to a certain power x ($P \propto ND^x$) that depends on the scattering domain (Rayleigh, Mie or Optics). Using a monodisperse PSD, the backscattered power recorded by VOLDORAD can be used to retrieve an estimate of the relative ejecta concentration within a cone of given aperture ϕ_w compared to the whole jet. Fig. 13(b) shows that for most of the Strombolian explosions, 80 per cent of the total particle load was included inside a dispersion cone 40° wide. Here again the systematic analysis shows a log-normal distribution of particle concentrations. These values are also in fair agreement, even if barely comparable in detail, with those inferred from photoballistic measurements carried out on one explosion at Stromboli in 1971 September. Indeed, Chouet *et al.* (1974) showed that 90 per cent of the total particle load was ejected within a dispersion cone 37° wide. Geometrical similarities found for explosions at Stromboli and Etna suggest that Strombolian explosions share a similar physical source mechanism.

6.4 Time evolution of the geometry of Strombolian explosions

In contrast, the same analysis on the timescale of about 1 hr revealed a large variability of Doppler spectra shapes, reflecting changing conditions of the source mechanism which produced the jet. Fig. 14 shows the time evolution of Doppler spectra shapes during the paroxysm (21:00 to 21:45 U.T.).

We observe two maxima in the occurrence of top-hat-shaped Doppler spectra events arising 15 and 45 min after the onset of the paroxysm, and two minima at about 0–5 and 30 min. Note that this trend seems to alternate with the occurrence of clearly oriented jets (triangular spectra). We suggest that top-hat Doppler spectra may occur when the magma column is high in the conduit, and sometimes partly filling the crater. In this case, overpressurized bubbles reaching the top of the magma column can expand more easily and then burst without physical constraints from the crater or

Downloaded from https://academic.oup.com/gji/article/183/3/1376/639331 by guest on 18 June 2021

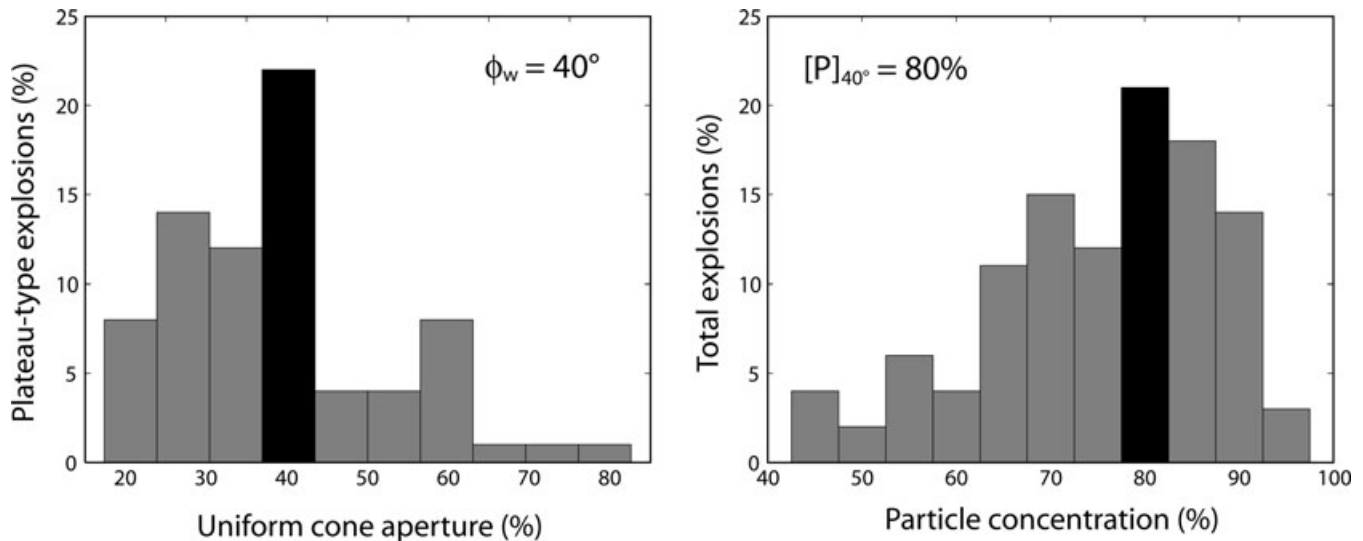


Figure 13. (a) Proportion of plateau-type Doppler spectra for strombolian explosions for different classes of cone apertures within which the ejecta distribution is uniform. (b) Proportion of the total number of explosions as a function of the relative concentration of particles comprised within a dispersion cone of $\phi_w = 40^\circ$.

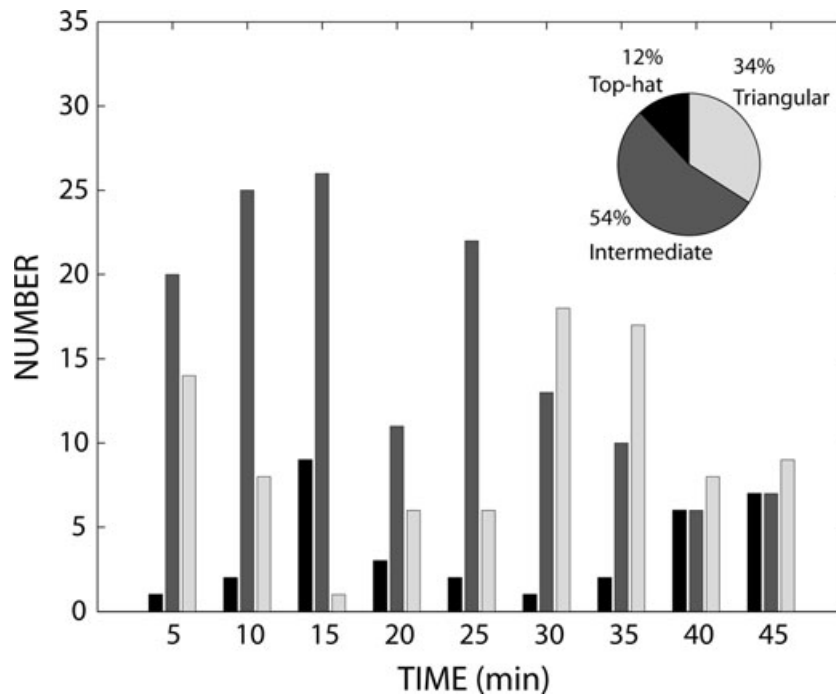


Figure 14. Time evolution of the distribution of Doppler spectra types during the paroxysm (21:00 to 21:45 U.T.) of the 2001 July 4 eruption at Etna SEC. Top-hat spectra (black) indicate entirely uniform ejecta distribution, triangular spectra (light grey) indicate oriented jets with non uniform ejecta distribution and intermediate spectra shapes (dark grey) indicate oriented jets with marked uniform ejecta distribution in the inner part of the cone.

conduit boundaries, leading more frequently to the hemispherical ejections of pyroclasts observed following the expansion of large lava bubbles above the crater rim. On the contrary, when the level of the magma column is low, gas slugs may burst deeper in the conduit, promoting vertically oriented jets. In this frame, the 30 min period may reflect cycles of variation of the magma column level, showing alternately minimum and maximum levels every 15 min.

However, intermediate and pure triangular Doppler spectra (i.e. vertically oriented jets.) are also observed when the magma column is high, suggesting that other physical mechanisms are involved

in the formation of these explosions. The shape of the gas pocket (spherical-bubble or slug-bubble), as well as its pressurization state, may control to the geometry of the jet. Also, the rheology of the magma stored in the lava lake, showing cooler lava mixing and recycled blocks, may also affect the geometry of the explosion. For instance, gas slug-bubbles are oriented vertically and might promote fairly upright ejection of lava clots, whereas, spherical-bubbles might lead to a rather uniform ejection. Secondary events such as bubble tails (impulsive burst) and wakes (foaming burst) could also explain some variability of jet geometry.

7 DISCUSSION AND CONCLUSIONS

Previous studies have already shown that VOLDORAD, our Volcano Doppler radar, is a powerful tool, which allows the routine retrieval of kinetic and loading eruptive parameters. This work carried out at Etna also shows some interesting geometrical features of Strombolian explosions which can be derived from radar measurements. This issue is particularly challenging because Strombolian explosions are very short-lived eruptions involving complex kinetic coupling and variable PSDs.

(1) We observed two distinct signatures in our Doppler radar spectra: top-hat-shaped spectra related to mainly uniform EADs (i.e. isotropic mass discharge, like hemispheric lava bubble outbursts), and triangular-shaped spectra related to Gaussian EADs (oriented jets).

(2) We carried out a statistical quantitative analysis in order to provide information on the eruption geometry of a large number of typical Strombolian explosions. We find that, at least at Etna, an opening angle of 40° is a statistically representative aperture for the part of the dispersion cone characterized by uniform ejection in Strombolian lava jets and that typical Strombolian explosions confine most of their ejecta (80 per cent) to within a relatively narrow (40°), vertically centred dispersion cone.

(3) The quantification of the geometrical features of Strombolian explosions can, in addition, provide constraints on shallow conduit processes. For instance, the time evolution of the top-hat Doppler spectra during the paroxysm suggests variations of the magma level over a 15 min timescale. Recent studies using thermal imagery (Bailey *et al.* 2006) and LIDAR (Favalli *et al.* submitted) measurements have also shown cyclic variation in the lava channel's volumetric flow rate that occurred over several hours of eruption at Mt Etna, suggesting that changes were taking place in the flow conditions up-channel, possibly at the vent.

Some assumptions included in both the ballistic and electromagnetic models are worth discussing in more detail. First, the law for gas velocity decrease used to obtain kinetic parameters is derived from a study carried out at Stromboli by Patrick *et al.* (2007) using FLIR imagery on a large number of Strombolian explosions. The decrease coefficient probably varies from one eruption to another; however, the accuracy of this method and the statistical number of events studied provide the basis for a good estimation of the gas behaviour for typical Strombolian activity. Additional thermal or UV measurements on different eruptions and volcanoes might serve to modify the constraints on the gas velocity decrease law. Secondly, given the complexity of scattering processes, the electromagnetic scattering model contains some assumptions to simplify it. In particular, particles are assumed to be compositionally homogeneous, spherical, and homogeneously distributed inside the sampling volume. Nevertheless, these effects are most probably balanced by the statistically high number of particles contained in a range gate, and they do not affect the significance of our geometrical results. Other concerns related to the radar data recording or processing may also arise locally because of imperfect automatic processing of aliased spectra or ground power echoes. Finally, geometrical results provided by the statistical analysis are based on the relation between the radial velocities and the jet aperture angles obtained. This relation was defined by a unique initial gas velocity ($V_0^g = 150 \text{ m s}^{-1}$) inferred from maximum velocities measured by the radar on a large number of Strombolian explosions that occurred during the paroxysm of this eruption, and from a single particle diameter ($D = 0.1 \text{ m}$), taken from the literature (see Section 6.1). These assump-

tions may lead to some uncertainties if each explosion were considered individually. However given our aim of a first order analysis of a long series of Strombolian explosions (~ 200), the average values taken here are most probably representative for typical Strombolian explosions at Etna.

The definition of Strombolian activity, mainly based on the source mechanism type, is quite ambiguous because of the large variety of surface eruptive expressions observed at different volcanoes. It has been suggested that Strombolian explosions originate from the collapse of a gas-rich foam layer at depth and the subsequent bubble coalescence that results in large gas slugs rising in the conduit, and bursting at the top of the magma column; hence, they would be responsible for the cyclical surface explosions (Jaupart & Vergnolle, 1988). However, the large variety of Strombolian explosion styles observed at the surface indicates additional shallow mechanisms at work. Patrick *et al.* (2007), in their work on Strombolian explosive styles using thermal measurements (FLIR), showed the existence of two main types: explosions dominated by coarse ballistic particles, and optically thick explosions having ash-rich plumes. This eruptive variability for a given vent and within a short timescale clearly emphasizes the contribution of additional processes in the uppermost conduit. Our study sheds light on the geometric variability of Strombolian explosions, which also has implications for the complexity of shallow conduit processes. We suggest in particular that the magma level may influence the ejection angle for the distribution of pyroclasts. A high magma column level would promote large and uniform EADs for explosions. In this case, overpressurized bubbles reaching the top of the magma column could expand more easily and then burst without physical constraints from the crater or conduit walls, leading more often to a hemispherical ejection of pyroclasts. For the opposite case, where the level of the magma column is low, gas slugs burst out deeper in the conduit, promoting vertically oriented jets. In addition, we think that the gas slug overpressure, the shape of the gas bubble, the rheological state of the lava pool and the way the overlying magmatic film breaks may also influence the geometry of the jet, which could explain the geometrical variability of Strombolian jets over a short timescale. Thus instabilities growing on the bubble surface, possibly causing the bubble to break, could develop locally, producing oriented lava jets, or on the whole bubble nose, generating much more hemispherical and uniform explosions. The shape of the gas pocket may also control the geometry of the jets. Gas slugs are typically oriented vertically and would promote a fairly vertical ejection of lava clots, whereas, spherical-cap bubbles would lead to a radial and uniform ejection of pyroclasts. This latter case is expected to occur especially when the magma column is high and partially fills the crater. The bubble can then equilibrate in an infinite liquid, which is not the case in the conduit, the bubble being constrained laterally. Finally, secondary events such as bubble tails and wakes must also be considered when explaining the variability of jet geometry. Bubble tails induce very sudden bursting episodes, most likely promoting high velocity and oriented jets, whereas bubble wakes generate foams of bursting bubbles, which limits the jet velocity (Vergnolle & Ripepe 2008).

The continuous radar recording we use here allowed, for the first time, a statistical quantitative analysis on the geometrical features of about 200 Strombolian explosions. Additional field experiments on other volcanoes should improve our knowledge of shallow Strombolian explosion mechanisms. Correlation with other geophysical methods should also reveal further interesting constraints on the processes at work. In particular, combining the current results with thermal measurements (FLIR) would be interesting to constrain the

velocity decoupling between gas and pyroclasts. In particular, the high spatial resolution of the FLIR imagery provides very valuable information on the gas evolution with height. Acoustic and seismic methods are also powerful tools which can be used to constrain shallow processes. The combination of these geophysical and remote sensing methods on common target volcanoes and the acquisition of simultaneous complementary datasets are highly desirable to improve our understanding of the dynamics of explosive volcanism and its transitions.

ACKNOWLEDGMENTS

This work was supported by a French MESR fellowship. Field work on Etna was possible thanks to the logistical help of INGV Catania and was funded by the CNRS-INSU PNRN programs 1999–2001. We gratefully acknowledge Georges Dubosclard, Roland Cordesses and Claude Hervier of the Observatoire de Physique du Globe de Clermont-Ferrand for the acquisition of the precious radar measurements without which that work could not have been achieved. We also thank Patrick Allard for his thoughtful comments on the PhD work and for providing video data, and Sylvie Vergnolle for extended discussions.

REFERENCES

- Bailey, J.E., Harris, A.J.L., Dehn, J., Calvari, S. & Rowland, S.K., 2006. The changing morphology of an open lava channel on Mt. Etna, *Bull. Volcanol.*, **68**, 497–515.
- Blackburn, E.A., Wilson, L. & Sparks, R.S.J., 1976. Mechanisms and dynamics of Strombolian activity, *J. Geol. Soc. (Lond.)*, **132**, 429–440.
- Bohren, C.F. & Huffman, D.R., 1983. *Absorption and Scattering of Light by Small Particles*, Wiley-Interscience, New York, 489pp.
- Chouet, B., Hamisevicz, N. & McGetchin, T. R., 1974. Photoballistics of volcanic jet activity at Stromboli, Italy, *J. geophys. Res.*, **79**, 4961–4976.
- Donnadiu, F., Dubosclard, G., Allard, P., Cordesses, R., Hervier, C., Kornprobst, J. & Lénat, J.-F., 2003. Sondages des jets volcaniques par radar Doppler: applications à l'Etna. Rapport quadriennal, *C.N.F.G.G.*, 1999–2002, pp. 119–124.
- Donnadiu, F. *et al.* 2005. Remotely monitoring volcanic activity with ground-based Doppler radar, *EOS, Trans. Am. geophys. Un.*, **86**(21), 201–204.
- Dubosclard, G., Cordesses, R., Allard, P., Hervier, C., Coltelli, M. & Kornprobst, J., 1999. First testing of a volcano Doppler radar (Voldorad) at Mt. Etna, *Geophys. Res. Lett.*, **26**, 3389–3392, doi:10.1029/1999GL008371.
- Dubosclard, G., Donnadiu, F., Allard, P., Cordesses, R., Hervier, C., Coltelli, M., Privitera, E. & Kornprobst, J., 2004. Doppler radar sounding of volcanic eruption dynamics at Mount Etna, *Bull. Volcanol.*, **66**, 443–456, doi:10.1007/s00445-003-0324-8.
- Formenti, Y., Druitt, T.H. & Kelfoun, K., 2003. Characterisation of the 1997 Vulcanian explosions of Soufrière Hills Volcano, Montserrat, by video analysis, *Bull. Volcanol.*, **65**, 587–605.
- Gouhier, M. & Donnadiu, F., 2006. Numerical modeling of Doppler radar signals of Strombolian eruptions, *Am. geophys. Un. Fall Meeting*, **V04**, 4177.
- Gouhier, M. & Donnadiu, F., 2008. Mass estimations of ejecta from Strombolian explosions by inversion of Doppler radar measurements, *J. geophys. Res.*, **113**, B10202, doi:10.1029/2007JB005383.
- Hort, M., Seyfried, R. & Voge, M., 2003. Radar Doppler velocimetry of volcanic eruptions: theoretical considerations and quantitative documentation of changes in eruptive behavior at Stromboli volcano, Italy, *Geophys. J. Int.*, **154**, 515–532, doi:10.1046/j.1365-246X.2003.01982.x.
- Jaupart, C. & Vergnolle, S., 1988. Laboratory models of Hawaiian and Strombolian eruptions, *Nature*, **331**, 58–60.
- McGetchin, T.R., Settle, M. & Chouet, B., 1974. Cinder cone growth modeled after Northeast Crater, Mount Etna, Sicily, *J. geophys. Res.*, **79**, 3257–3272.
- Métrich, N., Allard, P., Spilliaert, N., Andronico, D. & Burton, M., 2004. 2001 flank eruption of the alkali-and volatile-rich primitive basalt responsible for Mount Etna's evolution in the last three decades, *Earth planet. Sci. Lett.*, **228**, 1–17.
- Mie, G., 1908. Beiträge zur Optik trüber Medien, speziell kolloidaler Metallösungen, *Ann. Phys.*, **25**, 377–445, doi:10.1002/andp.19083300302.
- Mori, T. & Burton, M., 2009. Quantification of the gas mass emitted during single explosions on Stromboli with the SO₂ imaging camera, *J. Volc. Geotherm. Res.*, **188**, 395–400.
- Patrick, M., 2007. Dynamics of Strombolian ash plumes from thermal video: motion, morphology, and air entrainment, *J. geophys. Res.*, **112**, doi:10.1029/2006JB004387.
- Patrick, M.R., Harris, A.J.L., Ripepe, M., Dehn, J., Rothery, D.A. & Calvari, S., 2007. Strombolian explosive styles and source conditions: insights from thermal (FLIR) video, *Bull. Volcanol.*, **69**, 769–784.
- Ripepe, M., Rossi, M. & Saccorotti, G., 1993. Image processing of explosive activity at Stromboli, *J. Volc. Geotherm. Res.*, **54**, 335–351.
- Sauvageot, H., 1992. *Radar Meteorology*, Artech House Inc., Boston, 366pp.
- Steinberg, G.S. & Babenko, J.I., 1978. Experimental velocity and density determination of volcanic gases during eruption, *J. Volc. Geotherm. Res.*, **3**, 89–98.
- Vergnolle, S. & Brandeis, G., 1996a. Strombolian explosions: 1. A large bubble breaking at the surface of a lava column as a source of sound, *J. geophys. Res.*, **101**, 20 433–20 447.
- Vergnolle, S. & Ripepe, M., 2008. From Strombolian explosions to fire fountains at Etna Volcano (Italy): what do we learn from acoustic measurements?, *Geol. Soc. (Lond.)*, Special Publications, **307**, 103–124.
- Weill, A., Brandeis, G., Vergnolle, S., Baudin, F., Bilbille, J., Fèvre, J.F., Piron, B. & Hill, X., 1992. Acoustic sounder measurements of the vertical velocity of volcanic jets at Stromboli volcano, *Geophys. Res. Lett.*, **19**, 2357–2360.

APPENDIX A: DOPPLER SPECTRA MODELLING

A radar Doppler spectrum represents the power spectral density backscattered by objects, here pyroclasts, crossing the antenna beam, as a function of their radial velocities. Therefore, synthetic Doppler spectra can be constructed using (1) an electromagnetic scattering model that will compute the synthetic backscattered power and (2) a ballistic model that will compute the radial velocities of the particles.

A.1 Electromagnetic scattering model

Considering the wide range of particle diameters characterizing strombolian activity, the complete scattering theory is required to correctly account for the effects of large particles. A general solution of electromagnetic wave scattering was first described by Mie (1908). The application and computing solutions of this theory for plane waves scattered by spherical particles in a homogeneous medium was then developed by Bohren and Huffman (1983). For a monostatic horizontally polarized pulsed Doppler radar such as VOLDORAD, with negligible atmospheric attenuation at 23.5 cm wavelength, the synthetic power can be calculated as shown in Gouhier and Donnadiu (2008)

$$P_{\text{synth}} = \frac{C_r V_s \eta}{R^4}, \quad (\text{A1})$$

where C_r is the radar constant defined by a set of technical parameters related to the radar configuration, R is the slant distance from the antenna to the target, V_s the sampling volume and η the radar reflectivity. The latter depends on the target properties (number, size,

shape, composition, etc.), and can be calculated from the sum of the backscattering cross-section coefficients (σ_{bks}), per unit volume.

$$\eta = \sum_{i=1}^n \frac{\sigma_{bks}}{V_s}. \quad (A2)$$

The backscattering cross-section coefficients can then be calculated using the so-called Mie coefficient (a_n, b_n) over the sum of a convergent series

$$\sigma_{bks} = \frac{\lambda^2}{4\pi} \left| \sum_{n=1}^{\infty} (-1)^n (2n+1)(a_n - b_n) \right|^2. \quad (A3)$$

A.2 Ballistic model

Following Dubosclard *et al.* (2004), we assume that two forces are acting on a moving particle: the drag force (with a direction opposite to the velocity vector), and the gravitational force. Therefore, the position (x, z) of a particle at each time step can be calculated following:

$$\begin{aligned} \frac{d^2x}{dt^2} &= \left(\frac{3}{4} \frac{\rho_g}{\rho_p} \frac{C_D}{D} \right) (u_g - u_p) |w| \\ \frac{d^2z}{dt^2} &= \left(\frac{3}{4} \frac{\rho_g}{\rho_p} \frac{C_D}{D} \right) (v_g - v_p) |w| - g \end{aligned} \quad (A4)$$

with

$$|w| = \sqrt{(u_g - u_p)^2 + (v_g - v_p)^2}, \quad (A5)$$

where ρ_g and ρ_p stand for the gas and particle densities, respectively, C_D is the particle drag coefficient and D the particle diameter; u_g, u_p and v_g, v_p are the horizontal and vertical components of the gas and particle velocities, respectively. Eq. (A4) is integrated numerically by using a fourth order Runge–Kutta method. The initial velocity of a particle with a diameter D is taken as (Steinberg & babenko 1978):

$$V_0^p(D) = V_0^g - k\sqrt{D}, \quad (A6)$$

where V_0^g is the initial gas velocity and k is an empirical constant taken as 150, as inferred from previous studies (Chouet *et al.* 1974; Ripepe *et al.* 1993). The gas velocity decreases exponentially with height as follows:

$$V^g(z) = V_0^g \exp(-0.013z) \quad (A7)$$

A.3 Generation of synthetic Doppler spectra

Synthetic Doppler spectra are built by grouping together backscattered power and radial velocity values. The procedure can be summarized in three main steps:

- (1) *Step 1*: Calculation of the synthetic power [y -axis; Power] with PSD, EAD, V_0^g, t as inputs to the electromagnetic scattering model
- (2) *Step 2*: Calculation of the radial velocity [x -axis; V_p] with PSD, EAD, V_0^g, t as inputs to the ballistic model
- (3) *Step 3*: Construction of synthetic Doppler spectrum, using computed values of power and velocity (V_p) pairs found at steps 1 and 2, arranged by velocity classes.

The first and second steps are carried out simultaneously. Both require four input parameters: the PSD, the EAD, the initial gas velocity (V_0^g) and the time step (t). The power calculated from step 1 is used for the y -axis of the synthetic Doppler spectrum, and is expressed in dB (\log_{10} scale). The radial velocities of particles calculated from step 2 form the x -axis of the synthetic Doppler spectrum and are expressed in $m\ s^{-1}$. Results presented in this study were obtained using a typical time step of 0.1 s, and were focused on the range gate G_3 . When merging together power and radial velocity parameters from steps 1 and 2, respectively, the velocity range and number of velocity classes needed to be defined. The radial velocity range was usually defined as being between -100 and $100\ m\ s^{-1}$ and spanning 40 velocity classes (one class = $5\ m\ s^{-1}$).